

---

# A Multi-wavelength-based Method to de-project Gas and Dust Distributions of several Planetary Nebulae

Andrei Lințu<sup>1</sup>, Hendrik P. A. Lensch<sup>1</sup>, Marcus Magnor<sup>2</sup>, Sascha El-Abed<sup>1</sup>, Ting-Hui Lee<sup>3</sup>, and Hans-Peter Seidel<sup>1</sup>

<sup>1</sup> MPI Informatik, Saarbruecken, Germany [lintu@mpi.de](mailto:lintu@mpi.de), [lensch@mpi.de](mailto:lensch@mpi.de)

<sup>2</sup> TU Braunschweig, Germany [magnor@cs.tu-bs.de](mailto:magnor@cs.tu-bs.de)

<sup>3</sup> NOAO, Tucson, AZ, U.S.A. [thlee@noao.edu](mailto:thlee@noao.edu)

**Summary.** We describe a de-projection method to recover the 3D distribution of the ionized gas and dust component in planetary nebulae. Based on observations in the optical and radio regime, we propose an analysis-by-synthesis approach to obtain physically consistent spatial distributions that take extinction as well as scattering into account. As input we require two calibrated data sets of the same planetary nebula, a radio free-free emission map and a hydrogen recombination line map. From the radio free-free emission map, we first recover the density distribution of the ionized gas component using non-linear optimization while enforcing symmetry constraints. In a second step, we compare the recovered gas distribution to the input hydrogen recombination line map and optimize for the density distribution of the dust component considering extinction as well as scattering.

**Key words:** reconstruction, 3D modelling, volumetric modelling

## 1 Introduction

The importance of 3D models of planetary nebulae (PN) has increased lately. Ercolano and collaborators introduced the mocassin 3D Monte-Carlo photoionization code [1, 2] which is widely used in the literature for comparing models of PNe with observations. The results are very exact simulations using a given set of parameters, but have the major disadvantage that computations times are long and the parameters have to be adjusted by hand after every simulation run, until the results best match the observations [7].

A method to speed up 3D photoionization by interpolation was proposed by Morisset [8]. Due to the faster computation time this method would be more appropriate for automatic parameter optimization.

Another approach towards 3D modelling of PNe is presented by Steffen et. al [10]. The authors combine models generated by commercially available 3D modelling software with a custom renderer to reproduce observed data for given PNe.

Our approach is based on the algorithm presented previously by Magnor et al. [6], who reconstructed only 3D emissive volumes for planetary nebulae. The authors assume that absorption and scattering is negligible. As pointed out in [3, 4] there are, however, quite significant quantities of dust present in planetary nebulae and their effect needs to be considered. Therefore, we recover the 3D distribution of ionized gas *and* dust by extending the reconstruction algorithm in such a way that it also correctly accounts for absorption and scattering due to dust. In detail information about the proposed algorithm can be found in the paper focusing on computer graphics related technical details [5].

## 2 3D Reconstruction

Our reconstruction is based on the following rendering model. The observed radiance  $L(x, y)$  at a camera at position  $c$  is a function of the gas emission  $L_e(v)$ , extinction  $\tau(v)$ , and the albedo  $\sigma(v)$  of every voxel  $v$  along the ray through the camera pixel:

$$L(x, y) = \int_c^\infty e^{-\int_c^v \tau(w)dw} \cdot (L_e(v) + \sigma(v) \cdot S(v)) dv, \quad (1)$$

where  $S(v)$  is the total inscattering to the voxel  $v$  towards the camera due to the emission  $L_e^{star}$  of the nebula's central star(s) at position  $p^{star}$ . Considering single scattering only,  $S(v)$  is computed as

$$S(v) = \phi(c, v, p^{star}) L_e^{star} \cdot e^{-\int_{p^{star}}^v \tau(w)dw} \quad (2)$$

incorporating the extinction on the way from the star to the voxel as well as the Henyey-Greenstein scattering phase function  $\phi$  from the star to the voxel into the direction of the camera  $c$ . We assume the same phase function for all voxels.  $\phi$ ,  $L_e^{star}$ , and  $p^{star}$  are assumed to be known.

The extinction  $\tau(v)$  and the albedo  $\sigma(v)$  are directly proportional to the dust density  $d_{dust}(v)$ , while  $L_e(v)$  is linearly related to the concentration of ionized gas  $d_{gas}(v)$ . The exact factors can be found in physics textbooks. The goal is to determine  $d_{dust}(v)$  and  $d_{gas}(v)$  up to scale.

Reconstructing a 3D volume based solely on a single 2D view is generally an ill-posed problem. Using the axial symmetry constraint we can simplify the problem of reconstructing a 3D volume to that of reconstructing a 2D map. This reduces the complexity of the reconstruction problem and speeds up the optimization process. At each step in the reconstruction, a 3D volume is obtained from the 2D maps by rotating the maps around the symmetry axis. During the description of the algorithm, to better distinguish between reference images and the reconstructed 2D slices, we will refer to 2D recordings of real nebulae as *images*, and to the reconstructed 2D axis-symmetric distributions as *maps*.

### 2.1 Optimization

To drive our optimization we use the standard implementation of Powell's non-linear optimization method [9]. At every step, the sum of squared differences between the rendered and the reference image is evaluated. The algorithm minimizes this error

functional by updating individual pixels in the maps and stops when it drops below a given threshold. We always initialize the maps to be zero. Besides the values in the 2D map, the algorithm also optimizes the inclination and orientation angles of the nebula.

For a more efficient and more stable optimization we perform the optimization hierarchically, start by optimizing a low resolution map, successively increasing the resolution until it slightly exceeds the resolution of the input images.

## 2.2 Planetary Nebula Reconstruction

We use a pair of radio and visible wavelength images. The first input image (denoted as  $U$ ) is a radio continuum image from which we derive the gas distribution  $d_{gas}$ . The radio data is not affected by the dust distribution at all. The radio intensity  $U$  is related to the expected visible emission  $U'$  of the gas by the following equation [4]

$$U' = 6.85 \cdot 10^{-10} \cdot \nu \cdot U \quad (3)$$

where  $\nu$  is the frequency of the radio observation in  $GHz$  and  $U$  is measured in  $Jy$ . We compute  $U'$  which would correspond to an image of the nebula at the wavelength of  $H\alpha$  emission of the ionized gas as if no dust were present (Figure 1, left). The second input image, denoted  $A$  (Figure 2, left), is a captured image at this particular narrow band of visible wavelength corresponding to the same emissive  $H\alpha$  gas elements which in fact is affected by scattering and absorption due to the dust.

### Gas distribution estimation

In the first step, the *emission density map* corresponding to the ionized gas distribution  $d_{gas}(v)$  is reconstructed using  $U'$  as reference image. The rendering model simplifies to

$$L(x, y) = \int_c^\infty L_e(v) dv \quad (4)$$

because this observation is almost unaffected by the dust, so no absorption or scattering needs to be considered. The gas distribution map is estimated using the iterative non-linear optimization algorithm (Section 2.1). Given a current estimate of the gas density map  $d_{gas}$ , the emission  $L_e(v)$  is computed and an image is rendered according to Equation 4. The optimization drives the difference between this estimated image and the reference image  $U'$  to a minimum. We initialize the optimization with a homogeneous distribution. Figure 1 shows the reference image  $U'$ , the recovered gas density map  $d_{gas}$  and the rendering of the reconstructed volume. The reconstruction resembles the input up to the non-symmetries in the input.

### Dust distribution estimation

Using the gas density map  $d_{gas}$  from the previous step and the image  $A$  as reference, we optimize the *dust density map* until the reconstructed model resembles the reference image  $A$ . In this optimization step the nebula is rendered taking scattering and absorption into account as described by Equation 1. This time, the emission is derived from  $d_{gas}$ , while  $d_{dust}$  accounts for scattering and absorption. In this process, the emission density map  $d_{gas}$  recovered in step 1 is not optimized anymore. The results of this final optimization step are shown in Figure 2.

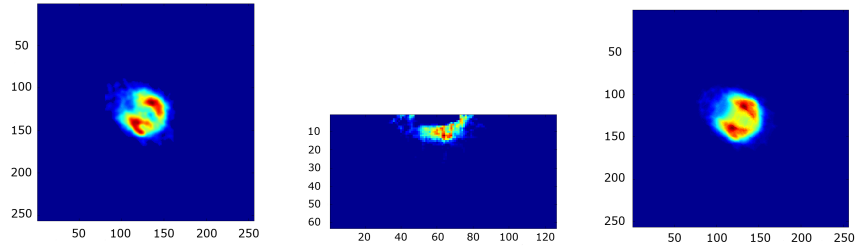


**Fig. 1.** Left: Input image for the M3-35 planetary nebula [4], corresponding to  $U'$ . Middle: Recovered gas density map  $d_{gas}$  (it is rotated along the top horizontal axis to obtain the rendering on right). Right: Rendering of the reconstruction, following Equation 4. We recover an inclination angle of  $73^\circ$ , orientation angle of  $62^\circ$ . Scale on the side shows pixels. In this Figure as well as in Figure 2 the rightmost renderings are obtained by rotating the map in the middle around the axis of symmetry with the determined inclination and orientation angle.

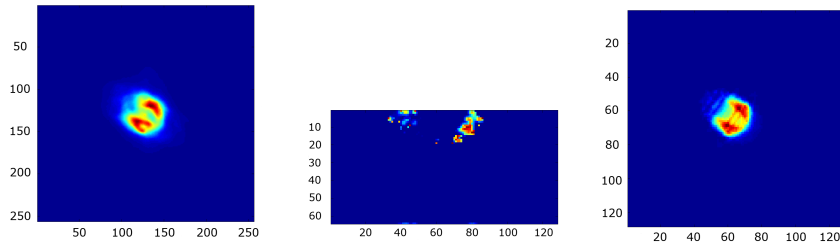


**Fig. 2.** Left:  $H\alpha$  image of the M3-35 planetary nebula [4], corresponding to A. The symmetry axis in this figure as well as in  $U'$  from Figure 1 spans from the upper left to the lower right corner. Middle: Final recovered  $d_{dust}$  dust map. Right: Rendering of the final reconstruction, considering absorption and scattering; gas and dust are rendered together at this step following Equation 1.

### 3 Conclusion

Given two input images at radio and visible wavelengths, we can recover both the 3D distribution of emitting gas as well as the density of dust particles in axis-symmetric nebulae. Our physically-based reconstruction and visualization algorithms simulate emission, absorption and scattering.

The approach presented in this paper only presents reconstruction results based on radio / visible input image pairs. In our more detailed, computer graphics oriented paper [5] another similar method is presented to reconstruct ionized gas and dust distribution starting from an infrared image at  $12 \mu m$  and a  $H\alpha$  image. In the mentioned paper reconstruction results for PN Hen 2-320 are reported.

Because we assume axial-symmetry, the reconstruction results depend on the inclination angle of the symmetry axis and the projection direction. The best quality is obtained if the symmetry axis is parallel to the image plane.

*Acknowledgement.* The authors are indebted to Kevin Volk, Gemini Observatory, for the provided infrared dataset (reconstruction results presented in [5]). We would also like to thank all other astronomers who kindly responded to our dataset requests, but whose data ended up not being used in the paper: Orla Aaquist, Yolanda Gomez, Luis Felipe Miranda and Jeremy Lim just to name some. This work has been partially funded by the Max Planck Center for Visual Computing and Communication (BMBF-FKZ01IMC01).

## References

1. B. Ercolano, M. J. Barlow, P. J. Storey, X.-W. Liu: MNRAS **340**, 1136 (2003)
2. B. Ercolano, M. J. Barlow, P. J. Storey: MNRAS **362**, 1038 (2005)
3. S. Kwok: *The Origin and Evolution of Planetary Nebulae* (Cambridge University Press 2000)
4. T.-H. Lee, S. Kwok: ApJ **632** 340 (2005)
5. A. Lințu, H. P. A. Lensch, M. Magnor et al: 3D Reconstruction of Emission and Absorption in Planetary Nebulae. In *IEEE/EG International Symposium on Volume Graphics*, ed by H-C. Hege, M. Raghu 2007
6. M. Magnor, G. Kindlmann, C. Hansen et al: Constrained Inverse Volume Rendering for Planetary Nebulae. In *Proc. of IEEE Visualization 2004* pp 83–90
7. H. Monteiro, H. Schwarz, H. E. Gruenwald et al: ApJ **620**, 321 (2005)
8. C. Morisset: Cloudy\_3D, a new pseudo-3D photoionization code. In *IAU Symposium*, ed by M. J. Barlow, R. H. Méndez 2006 pp 467
9. W. H. Press, S. A. Teukolsky, W. T. Vetterling et al: *Numerical Recipes in C: The Art of Scientific Computing* 2nd edn (Cambridge University Press 1992)
10. W. Steffen, J. A. López: RMxAA **42** 99 (2006)